Numerical Investigation of Optimization of Injection Angle Effects on Fluidic Thrust Vectoring

F. Forghany[1†], M. Taeibe-Rahni[2] and A. Asadollahi-Ghohieh[3]

*¹ Department of Mechanical and Aerospace Engineering, Science and Research Branch,
Islamic Azad University, Tehran, Iran*
² Department of Aerospace Engineering, Sharif University of Technology, Tehran, Iran
³ Civil Aviation Technology College, Tehran, Iran

†*Corresponding Author Email: farzad_forghany@yahoo.com*

ABSTRACT

A computational investigation was conducted to optimize the fluidic injection angle effects on thrust vectoring. Numerical simulation of fluidic injection for shock vector control, with a convergent-divergent nozzle concept was performed, using URANS approach with Spalart-Allmaras turbulence model. The fluidic injection angles from 60º to 120º were investigated at different aerodynamic and geometric conditions. The current investigation demonstrated that secondary injection angle is an essential parameter in fluidic thrust vectoring. Computational results indicated that, optimizing secondary injection angle would have positive impact on thrust vectoring performance. Furthermore, in most cases, decreasing expansion ratio of the nozzle with increasing NPR has negative impact on pitch thrust vector angle and thrust vectoring efficiency. That is, the highest pitch thrust vector angle is obtained by decreasing nozzle expansion ratio with increasing SPR in smaller fluidic injection angles. In addition, the current investigation attempted to initiate a database of optimized injection angles with different essential parameter effects on thrust vectoring, in order to guide the design and development of an efficient propulsion system.

NOMENCLATURE

A_e	nozzle exit area	$p_{t,s}$	secondary flow total pressure
A_t	nozzle throat area	p_∞	freestream static pressure
A_e/A_t	expansion ratio	SPR	secondary pressure ratio
CD	convergent-divergent	x_t	axial throat location
CFD	computational fluid dynamics	x/x_t	non-dimensional x coordinate
FTV	fluidic thrust vectoring	y^+	non-dimensional first cell height
F_x	axial component of thrust		
F_y	normal component of thrust	δ_p	pitch thrust vector angle, $\tan^{-1}$
h_t	throat height	φ	secondary flow injection angle
$\dot{m}_j$	primary (jet) mass flow rate	φ_n	normal to boundary injection angle
$\dot{m}_s$	secondary (slot) mass flow rate	φ_o	optimal injection angle
M_∞	freestream Mach number	η	thrust vectoring efficiency
NPR	nozzle pressure ratio		
$p_{t,j}$	primary flow total pressure		

1. INTRODUCTION

The development of an efficient propulsion system that is lightweight yet powerful enough to allow for flight is one of the key challenges in designing the next generation of launch vehicles. The propulsion system must also offer low-cost operations, improved reliability, and short turnaround times (Hanumanthroa *et al.*, 2011). Thrust vectoring is a candidate technology for the next generation aircrafts that may help satisfy take-off and landing requirements. Additionally, thrust vectoring could

augment conventional controls for some control power to trim the aircraft and thus reduce cruise trim drag. It can be a valuable control device at low dynamic pressures and post-stall high angles of attack, where conventional aerodynamic flights lose their power and effectiveness (Deere *et al.*, 2007).

Thrust vectoring technique is employed to control an aircraft's motion at low airspeeds and very high angles of attack, both of which are otherwise angles with unfeasible flight regimes (Wang *et al.*, 2016). It is applied to complement conventional aerodynamic flight control systems, to maximize the agility and safety of flight missions (Abdollahzadeh *et al.*, 2015). Thrust vectoring has established increasing applications in recent decade. Several thrust vector control concepts have been extensively investigated utilizing computational and experimental methods in the past (Páscoa *et al.*, 2013; Saghafi *et al.*, 2007; Gal-Or, 1990).

Two broad major methods have been employed to vector the exhaust gases of an engine. The conventional methods, relying on mechanical means and the most recent methods, which are fluidic-based thrust vectoring techniques (Kowal, 2002; Flamm, 1998). The fluidic thrust vectoring approach is based on using secondary air stream to deflect the primary jet. In contrast to the conventional mechanical thrust vectoring systems, fluidic systems require few or no moving parts (Cen *et al.*, 2015; Forghany *et al.*, 2015). Moreover, they result in a fast dynamic response compared to those achieved by mechanical actuators. These systems also reduce weight and complexity (Mason *et al.*, 2004; Strykowski *et al.*, 1997). All thrust vectoring techniques are evaluated with some common parameters such as: pitch thrust vector angle and thrust vectoring efficiency, which are important parameters to evaluate and compare the ability of different configurations to vector the primary exhaust flow with a given amount of secondary fluidic injection (Kowal, 2002; Flamm, 1996). The fluidic thrust vectoring techniques have been developed to include co-flow, counter-flow, shock vector control, throat skewing, and synthetic jet actuators (Jain *et al.*, 2015; Banazadeh *et al.*, 2008). All these vectoring techniques use secondary jet flows for thrust vectoring. Secondary jet injection in the main flow (primary) acts as an obstacle and source of the main flow momentum change (Zmijanovic *et al.*, 2012).
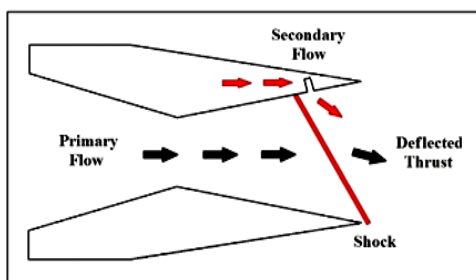

Fig. 1. Schematic of the shock-vector fluidic thrust vectoring.

The shock-vector control (SVC) method uses

supersonic flow turning through shocks created by fluidic injection in divergent section of a convergent-divergent nozzle (Zmijanovic *et al.*, 2016; Li, 2011; Jing-wei *et al.*, 2016; Jing-wei *et al.*, 2014). The primary flow interacts with the oblique shock wave and turns away from the longitudinal axis of the aircraft (Fig. 1).

Working best at off-design, over-expanded flow conditions, large thrust vector angles are generated via SVC techniques in expense of system thrust ratio as the flow is robustly turned and losses occur through shocks in the nozzle (Neely *et al.*, 2007; Ali *et al.*, 2012; Kostic *et al.*, 2015).

The present numerical study was an effort to establish a database of optimal fluidic injection angles with different effective parameter effects on thrust vectoring. The nozzle under investigation was a rectangular, convergent-divergent with different expansion ratio A_e/A_t=1.398, 1.796, and 2.195 (configurations I, II, and III). Moreover, the secondary flow with injection angles from 60° to 120° were achieved for predicting optimal nozzle performance in fluidic thrust vectoring (Fig. 2). Simulations were performed at nozzle pressure ratios of NPR=3.0 and 4.6, with different secondary pressure ratios (SPR) from 0.7 to 1.3, in pitch thrust vector angle, and thrust vectoring efficiency (conforming to secondary mass flow from 4% to 8% of the primary mass flow rate). In order to validate our computational method, a comparison between computational and experimental results (Waithe *et al.*, 2003) was performed.
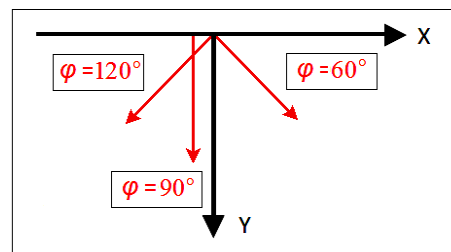

Fig. 2. Diagram of fluidic injection angle in the two dimensional (x-y plane).

2. COMPUTATIONAL METHODOLOGY

Our CFD code (PMB3D) has been developed and used as a predictor of internal nozzle performance and fluidic thrust vectoring, using convergent-divergent nozzle concept. The PMB3D requires a structured-mesh and a multi-block feature to allow the domain to be partitioned into different sections. This is critical for modeling complex configurations such as Convergent-Divergent nozzle, and for efficiently running the parallel version of PMB3D (Hojaji *et al.*, 2011; Forghany *et al.*, 2016). The explicit, finite volume flow solver represents the three-dimensional, unsteady, and Reynolds-averaged Navier-Stokes equations (Mannini *et al.*, 2010; Mary *et al.*, 2000). URANS equations were solved together with Spalart-Allmaras (S-A) one-equation turbulence model (Allmaras *et al.*, 2012; Spalart *et al.*, 1992). Based on previous studies,

Spalart-Allmaras and k-ε turbulence models have shown to be accurate popular for fluidic thrust vectoring simulations (Tian *et al.*, 2013; Zmijanovic *et al.*, 2012; Deere *et al.*, 2003). The Spalart-Allmaras (S-A) one-equation model provides the most stable results, which are favorably comparable to the experimental test. Some other researchers have chosen k-ε turbulence model requiring a wall function or a damping function. The one-equation Spalart-Allmaras (S-A) turbulence model was used here because of its simplicity, precision, robustness, and low computational cost (Deng *et al.*, 2015; Neely *et al.*, 2007; Mangine *et al.*, 2006). The inviscid flux terms were computed using a flux-vector splitting scheme, i.e., Advection Upstream Splitting Method Plus (AUSM+), which has several desirable properties such as providing exact resolution of contact interface and shock waves, being free of oscillations at stationary and moving shocks, and often results in a faster convergence rate (Chima *et al.*, 2003; Liou, 2001; Liou, 1996; Liou *et al.*, 1993). The MUSCL (Monotone Upstream-central Scheme for Conservation Laws) interpolation was used to achieve second-order accuracy with the Van Albada limiter to prevent spurious oscillations near shock waves. Also, an explicit 4th order Runge-Kutta scheme for time integration was implemented in each block (Birken, 2012; Hirsch, 1988; Rizzi *et al.*, 1973; Van Albada *et al.*, 1982).

The stagnation conditions were specified in the nozzle inlet and the fluidic injection port with a fixed total temperature (298. 5 K) and total pressure boundary conditions in respect to different NPR ($p_{t,j}/p_\infty$) and SPR ($p_{t,s}/p_{t,j}$). Also, the upstream far field boundary were defined with ambient pressure (101325 pa) and temperature (293.15 K) inflow condition. Moreover, a subsonic constant pressure outflow condition was used at downstream far field boundary, which switches to first order extrapolation if the flow is supersonic. A no-slip adiabatic wall condition was implemented on nozzle surfaces to obtain viscous solutions.

The nozzle used in this study was an axisymmetric, rectangular, and convergent-divergent nozzle from NASA Langley Research Center (Waithe *et al.*, 2003). The length of the nozzle was 115.57 mm, while the throat area of the nozzle was 2785.19 mm². In addition, height of the throat was 27.48 mm, and from throat to inlet was 57.78 mm. The base area ratio of the nozzle outlet to the throat (expansion ratio) was 1.796. The nozzle inlet center was set to be the origin of coordinates, the secondary inlet was located at 46.35 mm from injection slot to throat, while the width of slot was 2.032 mm (Fig. 3).

A comparison between three different quality meshes predicted static pressure distribution. The meshes, that were utilized consist of the total computational grid of 1,545,405 (coarse), 3,090,810 (medium), and 4,636,215 (fine), respectively. The comparison of the obtained results demonstrate that medium and fine meshes are very close and better than coarse mesh. Since the maximum difference in the static pressure

distribution (between the medium and fine meshes) is about 1.0% and the location of the main separation line is almost located at the same position for two different meshes. Thus, the computations were performed on the medium mesh to cut down the computational time (Fig. 4).
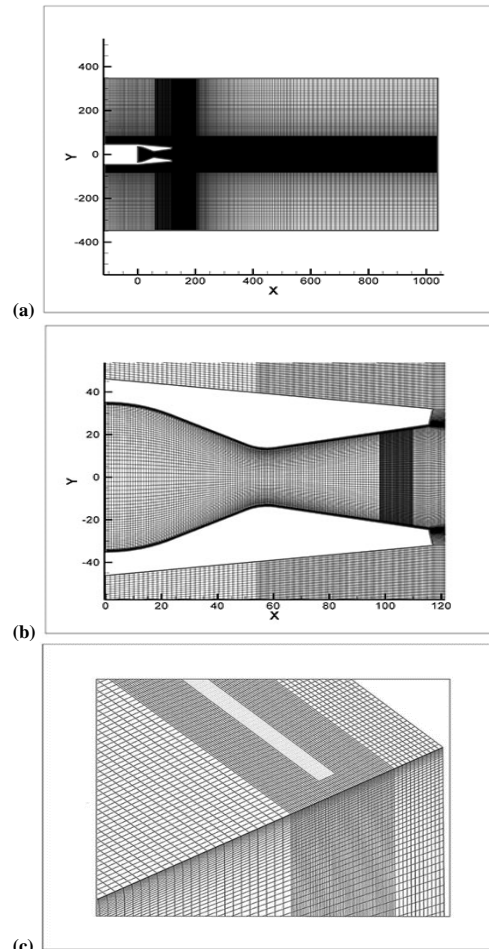

(a)

(b)

(c)

Fig. 3. The computational domain representing for: (a) Far-field and nozzle, (b) Close-up of nozzle, and (c) Close-up of injection slot.
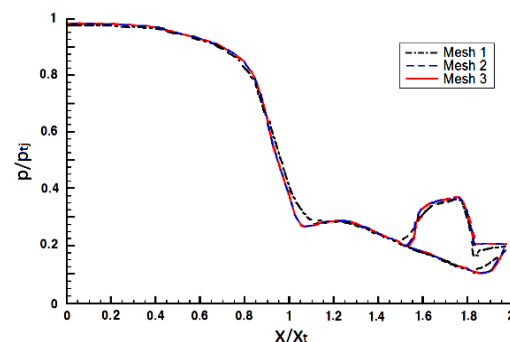

Fig. 4. Grid independence study at NPR=4.6 and SPR=0.7 using Spalart-Almaras (S-A) turbulent model.

The computational mesh was three-dimensional with 5 blocks defining the internal nozzle, 1 block representing the fluidic injection plenum, and 7 blocks representing the far field domain. The far

field was located 8 throat heights upstream and 34 throat heights downstream of the nozzle exit. The upper and lower lateral far field was located 25 throat heights above and below the nozzle. The first cell height in the boundary layer was defined for $y^+<1.5$ on all mesh spacing.

The computational results of this study were compared with the experimental results of Waithe *et al.* (2003). The centerline pressure distributions at nozzle pressure ratios of NPR=4.6 with secondary pressure ratio of SPR=0.7, is shown in Fig. 5. There was a significant correlation between our numerical results of pressure distributions along the upper and lower nozzle surfaces and the experimental results with a few exceptions near the shock. In this study, the shock location at the upper surface was predicted to be x/x_t=1.50 (x_t is axial location of the throat), while it was 1.53 and 1.61 in the experimental and PAB3D solver results, respectively. Additionally, our results at the lower surface gave x/x_t=1.87, compared to 1.89 and 1.95 found by the experimental and PAB3D results, respectively.
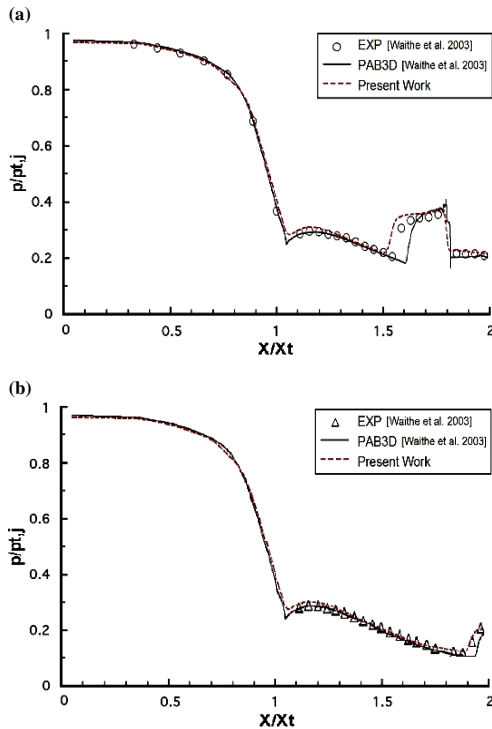

Fig. 5. Experimental and comptational pressures along internal nozzle, at NPR=4.6 and SPR=0.7 for: (a) upper wall and (b) lower wall.

3.   RESULTS

In this study, a computational investigation of secondary injection angle effects on fluidic thrust vectoring (FTV) was performed. To determine the pitch vector control and thrust vectoring efficiency, simulation of a rectangular convergent-divergent nozzle with shock-vector control method was achieved, using URANS approach and Spalart-Allmaras (S-A) one-equation turbulence model. The fluidic injection angles from 60° to 120° were

studied. Also, simulations were performed with effective parameters (NPR, SPR, expansion ratio, and fluidic injection angle) in thrust vectoring, at nozzle pressure ratios of NPR=3.0 and 4.6, with different SPR (0.7 to 1.3). In addition, nozzle design included different expansion ratios (configurations I, II, and III).

In the following sections, first the effect of NPR with secondary injection angle is presented. Then, effect of SPR with secondary injection angle, and the effect of nozzle expansion ratio with secondary injection angle are discussed, respectively.

3.1 Effect of NPR with Injection Angle

In order to understand the effect of fluidic injection angle with variable NPR in fluidic thrust vectoring, simulations were investigated at injection angles from 60° to 120º, with nozzle pressure ratios of NPR=3.0 and 4.6, and with different SPR. In addition, nozzle design included variable expansion ratio (Figs. 6-7).
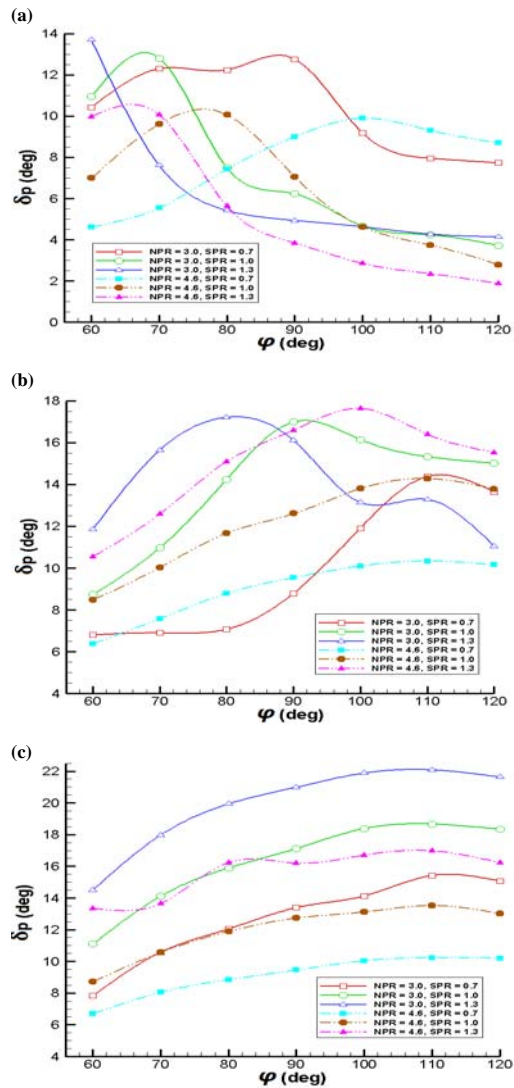

Fig. 6. Pitch thrust vector angles at different NPR, SPR, and fluidic injection angles for: (a) A_e/A_t=1.398, (b) A_e/A_t=1.796, and (c) A_e/A_t=2.195.

In most cases that were studied, decreasing nozzle pressure ratio has increased both pitch thrust vector angle and thrust vectoring efficiency. Moreover, in all configurations, the optimal fluidic injection angles compared to normal to boundary fluidic injection angle are also increased by decreasing NPR (with average improvements of about 61.8%, 64.5%, and 50.2%, respectively). It is the reducing effect of the induced oblique shock wave that reflects in opposite nozzle wall.
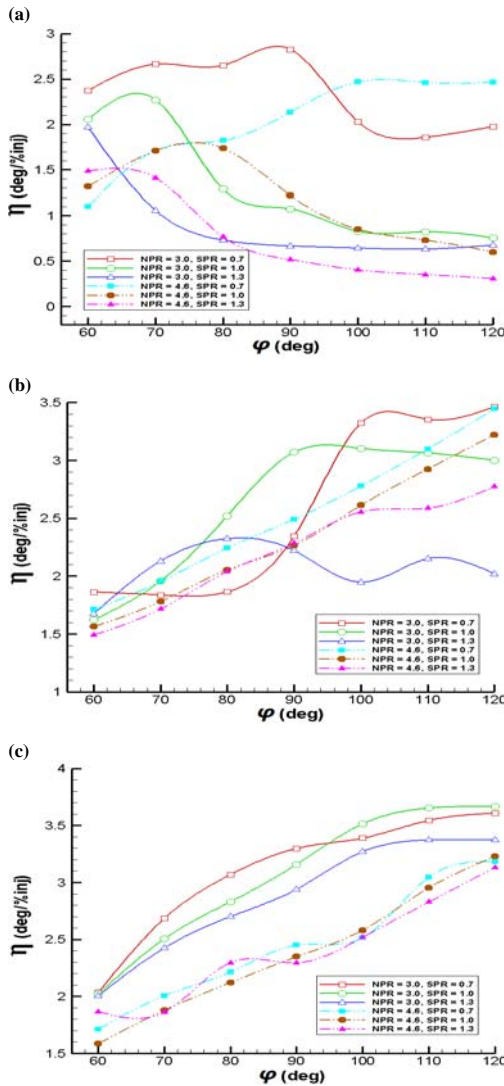

(a)

(b)

(c)

Fig. 7. Thrust vectoring efficiency at different NPR, SPR, and fluidic injection angles for:(a) A_e/A_t=1.398, (b) A_e/A_t=1.796, and (c) A_e/A_t=2.195.

Optimizing secondary flow injection angle with decreasing the mass flow rate of jet (primary) flow would cause the oblique shock or expansion waves of fluidic injection (secondary) flow become stronger. Also, the power of the oblique shock increases and the shock moves upstream. The total pressure of secondary flow is increased as the shock wave and flow separation from the upper wall moves further upstream. The influence of decreasing total pressure of primary flow and

increasing total pressure of secondary flow, has positive impact on pitch thrust vector angle and thrust vectoring efficiency. Improving pitch thrust vector angle is the result of the increase of pressure differential along nozzle walls (Fig. 8).

The thrust vectoring angle at NPR=3.0, with different SPR, and with optimal and normal to boundary fluidic injection angle compared to NPR=4.6 with unchanged condition has average improvement of about 27.44% and 18.85%, respectively. In addition, the thrust vectoring efficiency at NPR=3.0 compared to NPR=4.6 with similar condition has average improvement of about 14.63% and 15.93%, respectively (Table 1).

Finally, cases with the NPR=3.0 (which are achieved by optimal and normal to boundary injection angle), provide a better compromise for thrust vectoring angle and efficiency than the NPR=4.6 cases with constant condition. Additionally, the effect of decreasing total pressure of the nozzle flow has positive impact on pitch thrust vector angle and thrust vectoring efficiency.
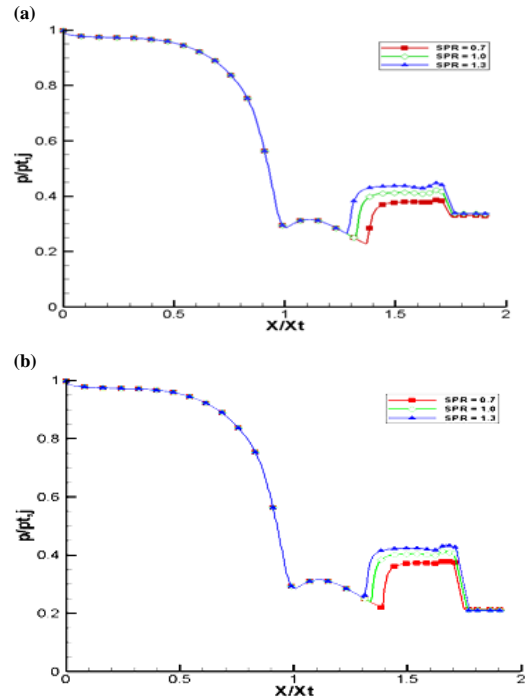

(a)

(b)

Fig. 8. Pressure distribution of upper surface along the nozzle (A_e/A_t=1.796) at different SPR with optimal fluidic injection angles for: (a) NPR=3.0 and (b) NPR=4.6.

3.2 Effect of SPR with Injection Angle

To identify the impact of fluidic injection angle with variable SPR in fluidic thrust vectoring, simulations were performed at injection angles from 60° to 120º, with secondary pressure ratios of (SPR=0.7, 1.0, and 1.3), and with different NPR. In this respect, nozzle design included variable expansion ratio (Figs. 6-7).

Increasing secondary nozzle ratio (SPR) with

Table 1 Effect of different conditions on nozzle performance with optimal and normal to boundary injection angles for: (a) A_e/A_t=1.398, (b) A_e/A_t=1.796, and (c) A_e/A_t=2.195.

Configuration I		Injection Angle (Optimal)			Injection Angle (Normal to Boundary)			Improvement	
NPR	SPR	φ_o (°)	δ_p (°)	η (°/%)	φ_n (°)	δ_p (°)	η (°/%)	δ_p %	η %
3.0	0.7	90	12.765	2.826	84.5	12.562	2.757	1.61	2.51
	1.0	70	12.806	2.271	84.5	6.858	1.177	86.7	92.9
	1.3	60	13.698	1.971	84.5	5.287	0.711	159.1	177.2
4.6	0.7	100	9.889	2.468	84.5	8.275	1.982	19.5	24.5
	1.0	80	10.057	1.738	84.5	8.536	1.471	17.8	18.1
	1.3	70	10.059	1.411	84.5	4.721	0.642	113.1	119.7

(a)

Configuration II		Injection Angle (Optimal)			Injection Angle (Normal to Boundary)			Improvement	
NPR	SPR	φ_o (°)	δ_p (°)	η (°/%)	φ_n (°)	δ_p (°)	η (°/%)	δ_p %	η %
3.0	0.7	110	14.379	3.555	78.9	7.053	1.854	103.8	80.9
	1.0	90	16.986	3.072	78.9	13.504	2.391	25.7	28.4
	1.3	80	17.209	2.324	78.9	16.453	2.217	4.59	4.82
4.6	0.7	110	10.329	3.099	78.9	7.578	2.151	36.3	44.1
	1.0	110	14.274	2.925	78.9	11.167	1.965	27.8	48.8
	1.3	100	17.626	2.555	78.9	14.391	1.961	22.4	30.2

(b)

Configuration III		Injection Angle (Optimal)			Injection Angle (Normal to Boundary)			Improvement	
NPR	SPR	φ_o (°)	δ_p (°)	η (°/%)	φ_n (°)	δ_p (°)	η (°/%)	δ_p %	η %
3.0	0.7	110	15.415	3.545	73.4	9.651	2.445	59.7	44.9
	1.0	110	18.661	3.653	73.4	13.985	2.476	33.4	47.5
	1.3	110	22.082	3.372	73.4	18.479	2.488	19.4	35.5
4.6	0.7	110	10.234	3.045	73.4	8.045	2.003	27.2	52.1
	1.0	110	13.522	2.952	73.4	10.791	1.912	25.3	54.3
	1.3	110	16.971	2.828	73.4	13.859	1.885	22.4	50.1

(c)

optimizing injection angle, in all cases studied, increased pitch thrust vector angle and decreased thrust vectoring efficiency. Increasing the mass flow rate of fluidic injection would strengthen the effects of oblique shock or oblique expansion waves. Also, the effective area in the nozzle is decreased by increasing secondary injection flow rate.

The strength of the oblique shock is increased and the shock moves upstream once SPR is increased. Thus, as SPR increases, the pressure distribution reinforces the increase of the pitch thrust vector angle. The shock and flow separation from the upper surface shift further upstream and subsequently, the flow reattaches as injection total

pressure is increased. The increasing of total pressure of the fluidic injection flow manifests improvement on pitch thrust vector angle and also shows weakening of thrust vectoring efficiency. The improvement of thrust vector angle and thrust vectoring efficiency by optimal injection angles are the results of the increased pressure differential along upper and lower walls (Figs. 9-10).

In some cases studied, increasing secondary nozzle ratio (SPR) with normal to boundary injection angle, decreased pitch thrust vector angle with a slighter rate. The decreasing in the rate of pitch thrust vector angle is explained by the influence of the induced oblique shock wave reflecting in opposite nozzle wall. The thrust vectoring angle at

secondary pressure ratios (SPR=0.7, 1.0, and 1.3), with different NPR, and with optimal fluidic injection angle compared to normal to boundary fluidic injection angle with unchanged condition has average increases of about 37.33%, 33.11%, and 33.41%, respectively. In addition, the thrust vectoring efficiency at different SPR (from 0.7 to 1.3), with optimal fluidic injection angle compared to normal to boundary fluidic injection angle with scheduled condition has average increases of about 39.01%, 38.51%, and 46.01%, respectively. Finally, the effect of increasing total pressure of the secondary flow injection with the optimal injection angle has positive impact on pitch thrust vector angle and thrust vectoring efficiency (Table 1)

3.3 Effect of Nozzle Expansion Ratio with Secondary Injection Angle

The nozzle performance needed to be optimized for NPR and Mach number ranges from low speed (take-off and landing) to high speed (cruise), for supersonic aircraft. However, thrust vectoring performance is compromised when the expansion ratio (exit area) is increased to meet higher NPR and Mach number requirements. In application, the aircraft designer would become selective about the nozzle designs to either maintain thrust efficiency while compromising on small units of thrust vectoring (e.g., at high speed) or to get the most thrust vectoring with some penalties in thrust efficiency (e.g., at low speed).
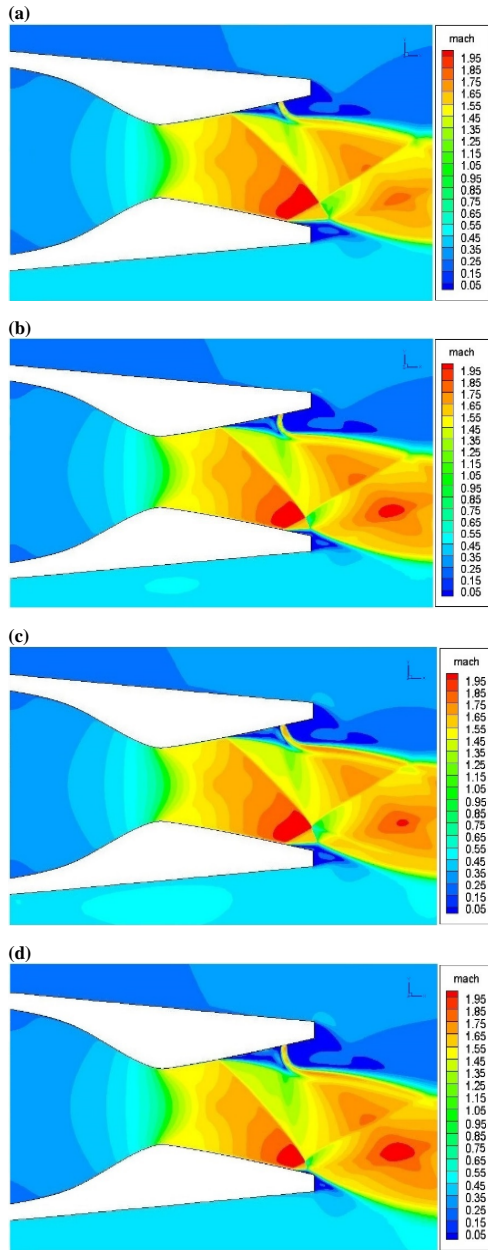

Fig. 9. Mach number shadowgraphs inside and outside the nozzle at NPR=3.0 with normal to boundary and optimal injection angles for: (a, b) SPR=1.0, (c, d) SPR=1.3.
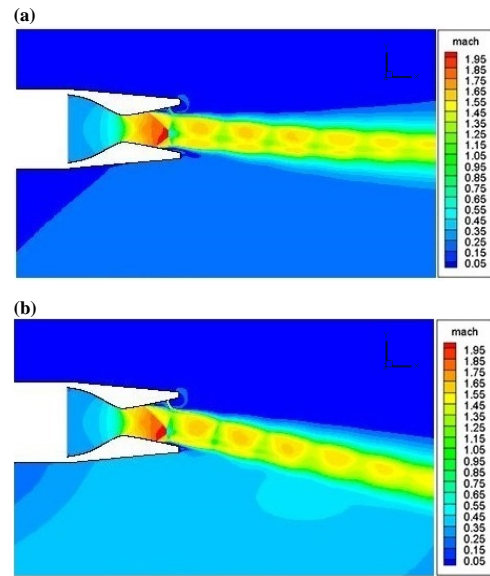

Fig. 10. Mach number shadowgraphs inside and outside the nozzle (A_e/A_t =1.796) at NPR=3.0, SPR=0.7: (a) normal to boundary injection angle, (b) optimal injection angle.

To understand the effects of fluidic injection angle with variable nozzle expansion ratio in vectored nozzle performance, simulations were achieved at injection angles from 60° to 120°, with nozzle pressure ratios of NPR=3.0 and 4.6, and with different SPR (0.7 to 1.3). In addition, nozzle design were performed at variable expansion ratio (A_e/A_t =1.398, 1.796, and 2.195) and with nozzle divergent angles of θ = 5.51°, 11.01°, and 16.59°, that comprised of configurations I, II, and III, respectively (Figs. 6-7).

In configuration I (A_e/A_t=1.398), the effect of fluidic injection (which is achieved by normal to boundary injection angle) in thrust vectoring performance is decreased slightly with increasing SPR. Once, SPR is increased, the induced oblique shock wave would reflect on opposite nozzle wall, when the oblique shock and the range of flow separation both decrease, except for the small SPR. The Convergent-Divergent nozzle configuration in the exit area could become oversized to compensate for the low speed and

provide the suitable mass flow for the engine. For this reason, the configurations II and III are utilized. The effects of fluidic injection in thrust vectoring performance improve with optimizing injection angle, decreasing NPR, and increasing SPR. The pitch thrust vector angle and thrust vectoring efficiency at configuration I (A_e/A_t=1.398), with nozzle pressure ratio of NPR=3.0 and 4.6, and with secondary pressure ratios of SPR=0.7, 1.0, and 1.3, as compared to optimal and normal to boundary fluidic injection angle have average increases of about 49.81% and 45.08%, respectively. Also, The thrust vectoring angle and thrust vectoring efficiency at configuration II (A_e/A_t=1.796), with different NPR and SPR, as compared to optimal and normal to boundary fluidic injection angle have average increases of about 29.44% and 38.21%, in turn. Moreover, The thrust vectoring angle and efficiency at configuration III (A_e/A_t=2.195), with equal condition, as compared to optimal and normal to boundary fluidic injection angle have average increases of about 29.51% and 46.83%, respectively (Table 1).
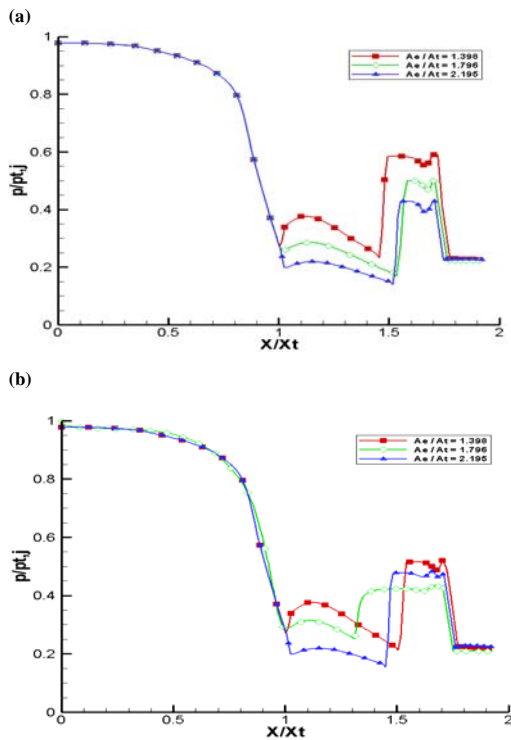

(a)

(b)

Fig. 11. Pressure distribution of upper surface along the nozzle at NPR=4.6, SPR=1.3, and with different expantion ratio for: (a) normal to boundary injection angles and (b) optimal injection angles.

On the whole, the nozzle with configuration III (A_e/A_t=2.195) at NPR=3.0 has the best end results considering all the employed configurations in thrust vectoring performance. The above mentioned outcomes are due to the increase of the nozzle total pressure that cause the shock wave and flow separation move further upstream. Moreover,

comparing all configurations at NPR=4.6, the nozzle with configuration II (A_e/A_t=1.796) performs significantly better in terms of thrust vectoring. The current improvement can be claimed to be the result of the increase of pressure differential along nozzle surfaces (Fig. 11).

Finally, increasing expansion ratio of nozzle with decreasing NPR, which is representative of most cases studied, has positive impact on pitch thrust vector angle and thrust vectoring efficiency. Also, increasing expansion ratio with increasing SPR, except for A_e/A_t=1.398 (achieved by normal to boundary injection angle), has positive effect on thrust vectoring performance. Moreover, increasing expansion ratio of nozzle with optimizing injection angle, which is representative of all cases studied, has positive impact on both pitch thrust vector angle and thrust vectoring efficiency (Fig. 12).
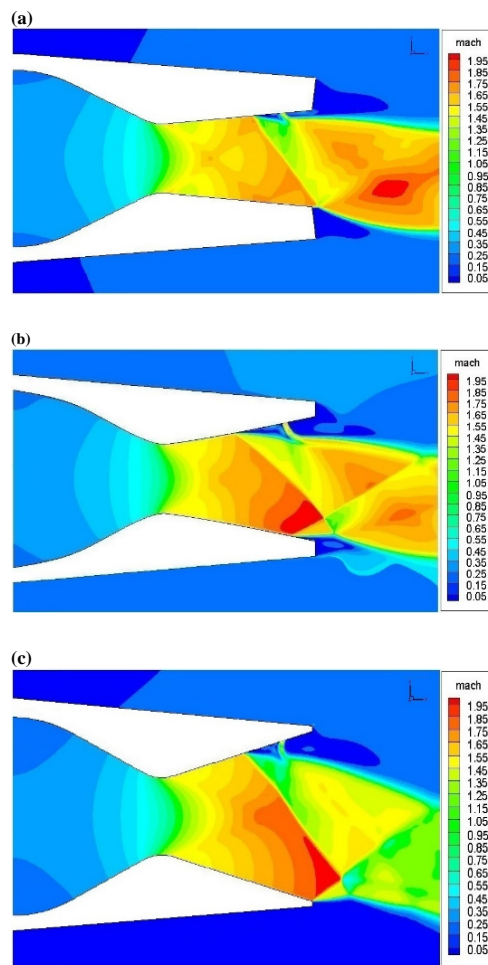

(a)

(b)

(c)

Fig. 12. Mach number shaowgraphs inside and outside the nozzle at NPR=4.6 with SPR=1.3, and with optimal injection angles for: (a) A_e/A_t=1.398, (b) A_e/A_t=1.796, and (c) A_e/A_t=2.195.

4. CONCLUSION

A computational investigation of fluidic injection angle effects on thrust vectoring (FTV) has been

conducted in the current study. The results can be of invaluable assistance in FTV optimization design and operation. In addition, the findings help the designer to develop a flow control system with better performance characteristics. The influence of effective parameters on fluidic thrust vectoring including nozzle pressure ratio, secondary pressure ratio, and fluidic injection angles varying from 60° to 120º were thoroughly investigated. Furthermore, nozzle design included different expansion ratios (A_e/A_t =1.398, 1.796, and 2.195).

The findings of the study have indicated that:

1. The secondary injection angle is an essential parameter in fluidic thrust vectoring,

2. in all cases, optimizing secondary injection angle would have positive impact on pitch thrust vector angle and thrust vectoring efficiency (by average increases of more than 44.76% and 53.14%, respectively),

3. in most cases, increasing NPR has negative impact on both pitch thrust vector angle and thrust vectoring efficiency over the range of the studied NPR (by average reductions of about 36.88% and 14.13%, respectively),

4. the effect of decreasing total pressure of nozzle (by decreasing NPR), would increase pitch thrust vector angle and thrust vectoring efficiency,

5. in most cases with constant NPR, increasing SPR would increase pitch thrust vector angle (with an average improvement of about 15.674%) and decrease thrust vectoring efficiency by decreasing the effective area in the nozzle (with an average decline of around 6.362%),

6. in most cases, increasing expansion ratio of the nozzle with decreasing NPR has positive impact on pitch thrust vector angle and thrust vectoring efficiency (by means of average increases of about 23.01% and 24.98%, respectively),

7. in most cases, the highest pitch thrust vector angle is obtained by decreasing expansion ratio of the nozzle with increasing SPR in smaller fluidic injection angles, and in most cases, the greatest pitch thrust vector angle is achieved by increasing expansion ratio of the nozzle with increasing NPR in higher fluidic injection angles.

REFERENCES

Abdollahzadeh, M., F. Rodrigues, J. C. Páscoa and P. J. Oliveira (2015). Numerical Design and Analysis of a Multi-DBD Actuator Configuration for the Experimental Testing of ACHEON Nozzle Model. *Aerospace Science and Technology* 41(1), 259-273.

Ali, A., G. Carlos, A. J. Neely and J. Young (2012, August). Combination of Thrust Modulation and Vectoring in a 2D Nozzle. In *proceeding of The 48th AIAA/ASME/SAE/ASEE Joint Propulsion Conference & Exhibit,* Atlanta, Georgia, AIAA Paper 2012-3780.

Allmaras, S. R., F. T. Johnson and P. R., Spalart (2012). Modifications and Clarifications for the Implementation of the Spalart-Allmaras Turbulence Model. In *proceeding of 7th International Conference on Computational Fluid Dynamics*, Hawaii.

Banazadeh, A., F. Saghafi, M. Ghoreyshi and P. Pilidis (2008). Experimental and Computational Investigation into the use of Co-Flow Fluidic Injection Effects on Fluidic Thrust Vectoring on a Small Gas Turbine. *The Aeronautical Journal* 112(1127), 17-25.

Birken, P. (2012, October). Optimizing Runge-Kutta Smoothers for Unsteady Flow Problems. *Electronic Transactions on Numerical Analysis* 39(1), 298-312.

Cen, Z., T. Smith, P. Stewart and J. Stewart (2015). Integrated Flight/Thrust Vectoring Control for Jet-powered Unmanned Aerial Vehicles with ACHEON Propulsion. In *proceeding of the Institution of Mechanical Engineers, Part G: Journal of Aerospace Engineering* 229(6), 1057-1075.

Chima, R. V. and M. S. Liou (2003). Comparison of the AUSM+ and H-CUSP schemes for turbo machinery applications. *NASA-TM 212457*.

Deere, K. A. (2003). Summary of Fluidic Thrust Vectoring Research Conducted at NASA Langley Research Center. In *proceeding of 21st AIAA Applied Aerodynamics Conference,* Orlando, Florida, AIAA Paper 2003-3800.

Deere, K. A., J. D. Flamm, B. L. Berrier and S. K. Johnson (2007). Computational Study of an Axisymmetric Dual Throat Fluidic Thrust Vectoring Nozzle for a Supersonic Aircraft Application. *American Institute of Aeronautics and Astronautics,* AIAA Paper 2007-5085.

Deng, R. and H. D. Kim (2015). A Study on the Thrust Vector Control Using a Bypass Flow Passage. *Journal of Aerospace Engineering* 229(9), 1722-1729.

Flamm, J. D. (1998). Experimental Study of a Nozzle Using Fluidic Counter Flow for Thrust Vectoring. . In *proceeding of The 34th AIAA/ASME/SAE/ASEE Joint Propulsion Conference and Exhibit,* Cleveland, OH, AIAA Paper 98-3255.

Forghany, F., M. Taeibe Rahni and A. Asadollahi (2016, May). Numerical Investigation of Active Flow Control in Fluidic Thrust Vectoring. *Submitted to Journal of Aerospace Engineering.*

Forghany, F., M. Taeibe Rahni and A. Asadollahi (2016, May). Numerical Investigation of Active Flow Control in Fluidic Thrust Vectoring. *Submitted to Proceedings of the*

Institution of Mechanical Engineers, Part G: Journal of Aerospace Engineering.

Forghany, F., M. Taeibe Rahni and A. Asadollahi Ghohieh (2015, November). Computational Investigation of Fluidic Injection Angle Effects on Thrust Vectoring. . In *proceeding of The 16th Fluid Dynamics Conference,* Iran.

Gal-OR, B. (1990). *Vectored Propulsion, Supermaneuverability and Robot Aircraft.* Springer-Verlage, New York.

Hanumanthrao, K., S. Ragothaman, B. A. Kumar, M. G. Prasad, and V. R. Sana Kumar (2011, January). Studies on Fluidic Injection Thrust Vectoring in Aerospike Nozzles. In *proceeding of AIAA Aerospace Sciences Meeting Including the New Horizons Forum and Aerospace Exposition*, Orlando, Florida, AIAA Paper 2011-293.

Heidari, M. R. and A. R. Pouramir (2016). Investigation and Comparison Effects of Fluid Injection Type in Thrust Vector Control. *Journal of Applied Fluid Mechanics* 9(1), 19-26.

Hojaji, M. (2011). *Investigation of the Flow over a Fin Located Downstream of a Supersonic Jet into Subsonic Cross-flow.* Ph. D. thesis, Sharif University of Technology, Tehran, Iran.

Jain, S., S. Roy, D. Gupta, V. Kumar and N. Kumar (2015). Study on Fluidic Thrust Vectoring Techniques for Application in V/STOL Aircrafts. *SAE Technical Papers* 2015-01-2423.

Jing-wei, S., W. Zhan-xue, Z. Xiao-Bo, Z. Li and S. Xiao-lin (2014). Performance Estimation for Fluidic Thrust Vectoring Nozzle Coupled with Aero-engine. In *Proceeding of 50th AIAA/ASME/SAE/ASEE Joint Propulsion Conference*, Cleveland, OH, AIAA Paper 2014-3711.

Jing-wei, S., Z. Li, W. Zhan-xue, and S. Xiao-lin (2016). Investigation on Flowfield Characteristics and Performance of Shock Vector Control Nozzle Based on Confined Transverse Injection. *Journal of Engineering for Gas Turbines and Power* 138(1).

Kostic, O. P., Z. A. Stefanovic and I. A. Kostic (2015). CFD Modeling of Supersonic Airflow Generated by 2D Nozzle with and without an Obstacle at the Exit Section. *Journal of FME Transactions* 43(2), 107-113.

Kowal, H. J. (2002). Advances in thrust vectoring and the application of flow control technology. *Canadian Aeronautics and Space Journal* 48(2), 145-151.

Li, L. (2011). *Numerical and Experimental Studies of Fluidic Thrust Vectoring Mechanisms.* Ph. D. thesis, Muroran Institute of Technology, Japan.

Liou, M. S. (1996). A sequel to AUSM; AUSM+. *Journal of Computational Physics* 129(1), 364-382.

Liou, M. S. (2001). Ten Years in the Making AUSM-family. *The 5th Computational Fluid Dynamics Conference sponsored by the American Institute of Aeronautics and Astronautics*, California, AIAA Paper 2001-2521.

Mannini, C., A. Soda and G. Schewe (2010, October). Unsteady RANS Modeling of Flow past a Rectangular Cylinder, Investigation of Reynolds Number Effects. *Computers and Fluids* 39(9), 1609–1624.

Mary, I., P. Sagaut and M. Deville (2000). An Algorithm for Unsteady Viscous Flows at All Speeds. *International Journal of Numerical Methods in Fluids* 34(5), 371-401.

Mason, M. S. and W. J. Crowther (2004). Fluidic Thrust Vectoring for Low Observable Air Vehicle. *The 2nd AIAA Flow Control Conference*, Portland, Oregon AIAA Paper 2004-2210.

Neely, A. J., F. N. Gesto, and J. Young (2007). Performance Studies of Shock Vector Control Fluidic Thrust Vectoring. In *Proceeding of the 43rd AIAA/ASME/SAE/ASEE Joint Propulsion Conference & Exhibit*, Cincinnati, OH, AIAA Paper 2007-5086.

Páscoa, J. C., A. Dumas, M. Trancossi, P. Stewart and D. Vucinic (2013, September). A Review of Thrust Vectoring in Support of a V/STOL Non-Moving Mechanical Propulsion System. *Central European Journal of Engineering* 3(3), 374-388.

Saghafi, F. and A. Banazadeh (2007). Investigation on the Flight Characteristics of a Conceptual Fluidic Thrust-Vectored Aerial Tail-Sitter. In *Proceedings of the Institution of Mechanical Engineers, Part G: Journal of Aerospace Engineering* 221(5), 741-755.

Spalart, P. and S. Allmaras (1992). One-equation Turbulence Model for Aerodynamic Flows. *30th Aerospace Sciences Meeting and Exhibit.* Reno, NV, AIAA Paper 92-0439.

Strykowski, P. J., G. F. Schmid, F. S. Alvi and A. Krothaplli (1997). Vectoring Thrust Using Confined Counter Current Shear Layers. In *Proceeding of AIAA 28th Fluid Dynamics Conference*, Snowmass Village, CO.

Tian, C. and L. Yijia (2013). Turbulence Models of Separated Flow in Shock Wave Thrust Vector Nozzle. *Engineering Application of Computational Fluid Mechanics* 7(2), 182-192.

Van Albada, G. D., B. Van Leer and W. W. Roberts (1982). A Comparative Study of Computational Methods in Cosmic Gas Dynamics. *Astronomy and Astrophysics* 108(1), 76-84.

Waithe, K. A. and K. A. Deere (2003). Experimental and Computational Investigation

of Multiple Injection Ports in a Convergent-divergent Nozzle for Fluidic Thrust Vectoring. In *Proceeding of 21ˢᵗ AIAA Applied Aerodynamics Conference*, Orlando, Florida, AIAA Paper 2003-3802.

Wang, Y. and D. Wang (2016, January). Research on variable thrust directional control technique for plateau unmanned aerial vehicles. *Science China Information Sciences* 59(2), 1-4.

Zmijanovic V., L. Leger and E. Depussay (2016).

Experimental-Numerical Parametric Investigation of a Rocket Nozzle Secondary Injection Thrust Vectoring. *Journal of Propulsion and Power* 32(1), 196–213.

Zmijanovic, V., L. Leger and V. Lago (2012). Experimental and Numerical Study of Thrust-Vectoring Effects by Transverse Gas Injection into a Propulsive Axisymmetric C-D Nozzle. In *Proceeding of 48th AIAA/ASME/SAE/ASEE Joint Propulsion Conference & Exhibit*, Atlanta, Georgia, AIAA Paper.2012-3874.